ACS OMEGA

Article

Cite This: ACS Omega 2017, 2, 7275-7280

http://pubs.acs.org/journal/acsodf

Surface Zeta Potential and Diamond Seeding on Gallium Nitride Films

Soumen Mandal,*[,†] Evan L. H. Thomas,[†] Callum Middleton,[§] Laia Gines,[†] James T. Griffiths,[∥] Menno J. Kappers,[∥] Rachel A. Oliver,[∥] David J. Wallis,[‡,∥] Lucy E. Goff,[⊥] Stephen A. Lynch,[†] Martin Kuball,[§] and Oliver A. Williams*[,†]

[†]School of Physics and Astronomy and [‡]School of Engineering, Cardiff University, Cardiff CF24 3AA, U.K.

[§]Center for Device Thermography and Reliability, University of Bristol, Bristol BS8 1TL, U.K.

[∥]Department of Materials Science and metallurgy, University of Cambridge, Cambridge CB3 0FS, U.K.

[⊥]Department of Physics, University of Cambridge, Cambridge CB3 0HE, U.K.

ABSTRACT: The measurement of ζ potential of Ga-face and N-face gallium nitride has been carried out as a function of pH. Both of the faces show negative ζ potential in the pH range 5.5−9. The Ga-face has an isoelectric point at pH 5.5. The N-face shows a more negative ζ potential due to larger concentration of adsorbed oxygen. The ζ potential data clearly showed that H-terminated diamond seed solution at pH 8 will be optimal for the self-assembly of a monolayer of diamond nanoparticles on the GaN surface. The subsequent growth of thin diamond films on GaN seeded with H-terminated diamond seeds produced fully coalesced films, confirming a seeding density in excess of 10^{11} cm^{-2}. This technique removes the requirement for a low thermal conduction seeding layer like silicon nitride on GaN.

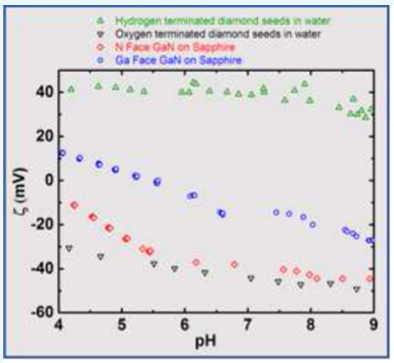

Zeta potential of Ga and N face Gallium nitride as a function pH compared with zeta potential of H and O-terminated diamond particles in water. The positively charged H-terminated seed solution facilitates the assembly of monolayer of diamond seeds on the GaN surface.

1. INTRODUCTION

With the high breakdown voltage and current handling ability, gallium nitride (GaN) high electron mobility transistors (HEMTs) are the current benchmark for high-power, high-frequency applications.[1,2] However, the heat generated during high power density conditions limits the use of such devices, with Lee et al.[3] demonstrating that small increases in the operating temperature can lead to drastic reductions in the device lifetime. To realize long lifetime and high performance of GaN electronics, it is therefore essential to effectively extract heat from the devices. At present, for effective thermal management, the structures are fabricated from GaN grown on top of SiC substrates[4,5] and are widely used for radio frequency applications due to their superior thermal conductivity ($\kappa_{SiC} \approx 360-490$ W/m K[6]). The use of SiC has allowed good device performance in terms of thermal management, but by replacing SiC with diamond substrates of thermal conductivity up to $\kappa_{Diam} \approx 2100$ W/m K,[7] more significant advances in GaN electronic devices will be possible.

To fabricate GaN on diamond devices, the diamond can either be grown on top of the GaN or vice versa. Although previous trials of GaN grown on single crystal diamond have led to promising results,[8,9] the high cost associated with single crystal diamond makes this technique unattractive. Alternatively, polycrystalline diamond can be grown on GaN through the use of an adhesion layer.[10,11] However, although the polycrystalline diamond has excellent thermal properties,[12] the poor thermal conductivity of the typically amorphous adhesion layer presents a barrier to the extraction of heat from the devices.[13] Therefore, it is crucial to grow the diamond layer directly on to the surface of the GaN to provide more effective thermal management. Initial attempts have been made with mixed success.[14−16] A further complication for the case of diamond growth on GaN is that wurtzite GaN has two distinct terminations along the polar direction. For (0001) GaN, the surface is Ga-terminated, and for the $(000\bar{1})$ surface, the GaN is N-terminated. In the majority of cases GaN HEMT layers are grown on the Ga-face, and therefore the diamond heat spreading layer must be produced on the back N-face. Because the GaN crystal is polar along the [0001] axis, it might be expected that the different crystal surfaces could have very different charge states, and therefore understanding diamond film nucleation on the appropriate face is vital.

Because of large differences in surface energies between diamond (~6 J/m^2)[17] and the most commonly used Si (1.5 J/m^2)[18] substrates for diamond growth, attempts at hetero-epitaxial diamond growth usually result in sparse, isolated diamond islands, with densities of 10^4-10^5 cm^{-2} for growth on

Received: July 26, 2017
Accepted: October 6, 2017
Published: October 27, 2017

DOI: 10.1021/acsomega.7b01069
ACS Omega 2017, 2, 7275−7280

silicon. Hence, a seeding technique is needed to realize coalesced diamond thin films on foreign substrates. With a similar large difference in the surface energy[19] between diamond and GaN with a value of ~2 J/m^2, a seeding technique is also then required for diamond thin-film growth on this compound. Historically, a variety of seeding techniques have been used to grow diamond on nondiamond substrates from mechanical abrasion with diamond grit to bias enhanced nucleation.[20] In this work, we have determined the ζ potential of both Ga-face and N-face GaN. The result has been used to select the most suitable diamond particle for seeding the GaN wafers, leading to self-assembly of the monolayer of diamond nanoparticles. The seeded wafers have also been imaged using atomic force microscopy (AFM) to detect the effectiveness of the seeding. Finally, the wafers with both types of seeds were exposed to diamond growth conditions to grow thin diamond films on GaN.

2. RESULTS AND DISCUSSION

Figure 1 details the ζ potential of the Ga-face and N-face GaN surface as a function of pH. The ζ potential for N-face GaN is

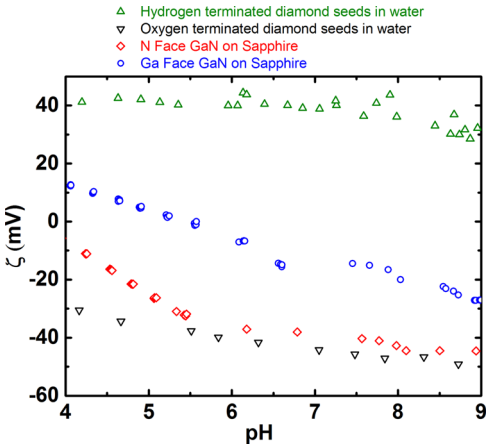

Figure 1. ζ Potential vs pH curve for Ga-face and N-face GaN, hydrogen and oxygen-terminated diamond seeds in water are shown. The hydrogen-terminated seeds show positive ζ potential in the pH range 4−9, the Ga-face GaN has an isoelectric point at pH ~ 5.5, and rest of the materials show varying degrees of negative ζ potential. The data for the seeds have been taken from Hees et al.[27]

negative and there is moderate variation in the potential as the pH changes from 4 to 9. A similar trend is seen for Ga-face GaN, which has an isoelectric point at pH ~5.5 with negative ζ potential at higher pH values. With water being the solvent for the diamond nanoparticle seeding solutions, the main region of interest for diamond growth are the values in the pH range 6−7. In this range, N-face GaN shows a more negative ζ potential when compared to that of Ga-face GaN. This can be attributed to two different causes: (i) there is a presence of higher concentration of adsorbed oxygen on the N-face GaN,[21,22] and (ii) the Ga-face GaN surface is generally smoother than the N-face GaN surface,[23] as is evident from the AFM images in panels (A) and (E) in Figure 2 leading to a minor inaccuracy in the calculation of the total surface area in contact with the streaming electrolyte. Foster et al.[24] have shown that under aqueous conditions, the N-face of GaN oxidizes more rapidly than that of the Ga-face. The effect of oxidation of activated carbon on ζ potential was studied by Chingombe et al.,[25] with

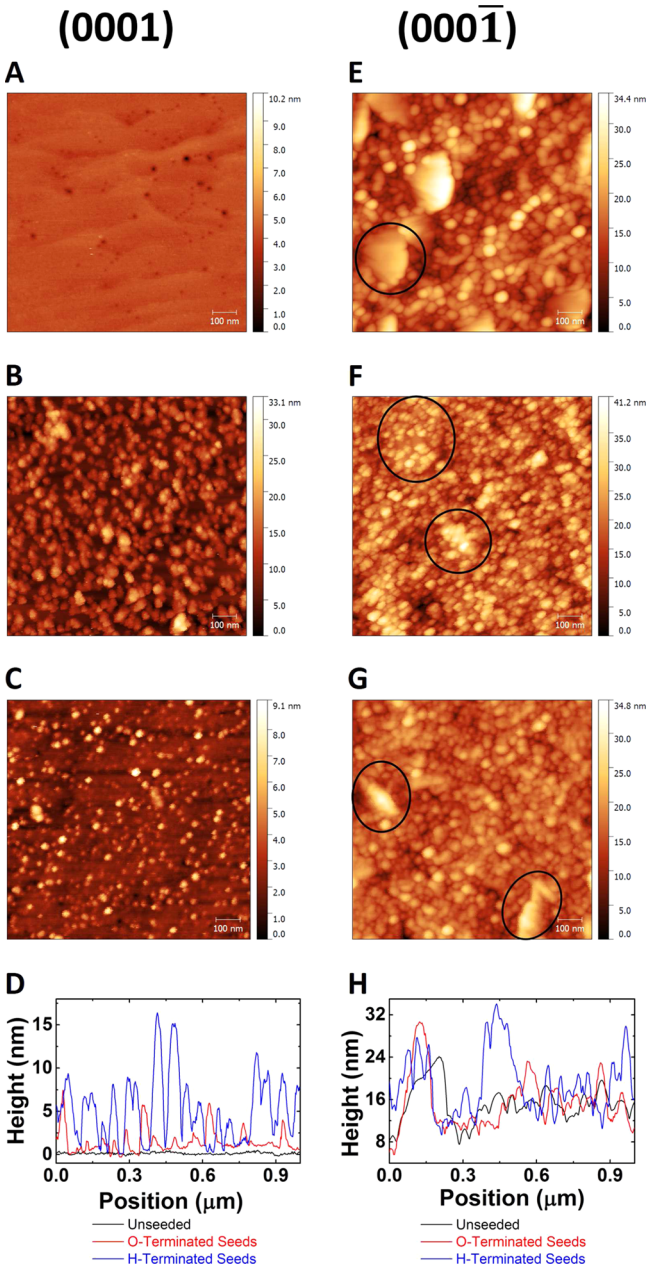

Figure 2. AFM images of seeded and unseeded Ga-face and N-face GaN. The left-hand side (panels (A)−(D)) shows images from Ga-face GaN, whereas the right-hand side (panels (E)−(H)) corresponds to N-face GaN. Panels (A) and (E) are for the respective unseeded GaN. Panels (B) and (F) show the surface after seeding with H-terminated seeds. Panels (C) and (G) show the GaN surfaces after seeding with O-terminated seeds. Panels (D) and (H) are the line profiles of unseeded and seeded surfaces for both types of GaN.

the authors finding that the higher the oxygen content on the surface of activated carbon, the more negative was the ζ potential at a given pH value. A similar trend can be seen for hydrogen and oxygen-terminated nanodiamonds as well, the ζ potential versus pH for which have been plotted in Figure 1. The oxygen-terminated seeds show negative ζ potential for the whole pH range, whereas hydrogen-terminated seeds have a positive ζ potential in the same range. For self-assembly of a monolayer of nanodiamonds on the GaN surface, it is important to have the GaN and seed ζ potential of opposite polarities with the highest possible difference. The results from

DOI: 10.1021/acsomega.7b01069
ACS Omega 2017, 2, 7275−7280

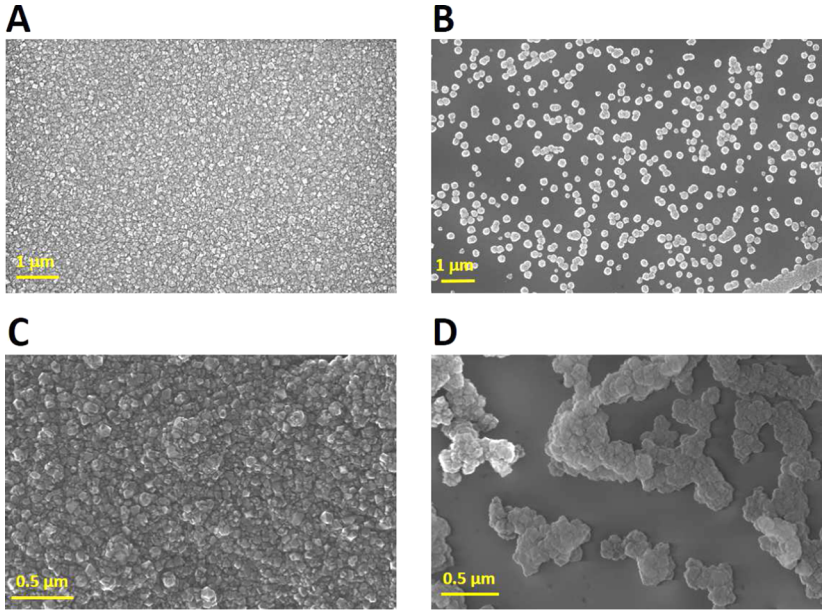

Figure 3. SEM image of diamond thin films grown on GaN. Panel (A) shows the growth on surface treated with H-terminated diamond seeds while Panel (B) shows the sample treated with O-terminated seed solution on the Ga-Face of GaN. Panel (C) is the image for diamond growth on H-terminated diamond seeds treated N-face of GaN. Panel (D) shows growth for O-terminated seed treated N-face GaN showing noncoalesced growth.

the ζ potential study of the GaN surface and diamond seeds show that such conditions are met when the seeds are H-terminated and the pH of the solution is close to 8. Another interesting feature to note in the ζ potential is the change in the potential as the pH is changed. Foster et al.[24] have shown that as the GaN surface is exposed to higher pH, the oxygen content of the surface increases, which can lead to a more negative ζ potential. On the other hand, exposure to aq HCl leads to chlorine chemisorption, which lowers oxide content[26] on the surface, resulting in lower negative ζ potential and eventually an isoelectric point on the Ga-face GaN.

To compare the effectiveness of the seeding solutions, AFM was performed on seeded and unseeded GaN surfaces, with the results shown in Figure 2. Panels (A) and (E) of Figure 2 show the AFM image of unseeded surfaces of Ga-face and N-face GaN. The second panel on both sides of the figure (panels (B) and (F)) shows the sample surface after being seeded by H-terminated diamond seeds. Although the seeds are clearly visible on the smooth Ga-face GaN surface, the same is not so clearly obvious for N-face GaN. The reason is the surface roughness of this surface. However, focusing on the larger crystallites on the surface in both figures (marked on the images) it can be seen that although in panel (E) the crystallites are completely exposed, similar crystallites in panel (F) show evidence of being covered by a conformal layer of particles. Comparing these small particles with the ones discernible in panel (B), it is quite clear that there is a very high density of nanodiamond particles also on this surface. In addition, pieces of both the Ga-face and N-face wafers were seeded with the O-terminated seeds. The AFM images of such samples are shown in panels (C) and (G) of Figure 2. On the Ga-face surface, a direct comparison between panels (B) and (C) shows that the O-treated seeds produce a less densely seeded surface than the H-terminated seeds. The N-face surface requires a similar approach as that taken for the H-terminated seeds, considering the AFM images on larger crystallites present on the surface. The large crystallites on panel (G) show clear faceting, and the usual granularity introduced by seeds is missing. Finally, to compare more closely the three surfaces (unseeded and H- and O-terminated seeded) for both types (Ga-face and N-Face) of material, we have taken a line profile from the AFM data. The plots are shown in panels (D) and (H). The Ga-face surface (panel (D)) is very easy to interpret. The unseeded line profile is presented in black and shows the presence of no peaks or valleys. The O- and H-terminated seeded surfaces are presented in red and blue, respectively. Although the blue curve shows large number of peaks ranging between 4 and 16 nm, the number of peaks for the red curve is much lower, showing a reduced seeding density. For comparing the surfaces of N-face GaN, we have purposely taken the line profiles in such a way that at least one crystallite falls in the profile for each surface. As before, the unseeded surface is plotted in black, O-terminated seeded surface in red, and H-terminated surface in blue. For all three curves, there is a peak between positions 0 and 0.2 μm. Although for unseeded and O-terminated nanodiamond-treated surfaces we do not see any subfeatures in the peak, clear subfeatures can be seen on the H-terminated nanodiamond-treated surface. This clearly shows that although H-terminated seeds produce a high density of seeds on the surface, the O-terminated seeds fail to do so, in line with the ζ potential measurements of the substrates. From Figure 2, it is therefore clear that H-terminated nanodiamond seed solution is the best option for creating a high-density seeded surface in both types of GaN. In the literature, the evidence of surface modification of substrates by chemical precursors can be found, which leads to nucleation without modification of detonation nanodiamonds,[28] but this technique leads to inclusion of an additional step in the growth process.

Finally, to test the effectiveness of seeding with H-terminated seeds, diamond thin films were grown on seeded (H-terminated and O-terminated) GaN. The scanning electron microscopy (SEM) images of the grown films were taken, and the results are shown in Figure 3. Panels (A) and (C) in the figure show the growth on GaN treated with H-terminated diamond seed

DOI: 10.1021/acsomega.7b01069
ACS Omega 2017, 2, 7275−7280

solution for Ga-face and N-face, respectively. We can see a complete pinhole-free film, indicating a seeding density greater than 10^{11} cm^{-2}. Panels (B) and (D) in the same figure show the samples treated with O-terminated diamond seed solution for Ga-face and N-face, respectively. In this case, only isolated crystals can be seen for Ga-face. Similarly, for N-face, we see noncoalesced growth. The growth that is seen on the N-face can be attributed to the presence of initial surface roughness, which can generate spontaneous nucleation sites[29,30] but with low site density. So, from these figures it is clear that O-terminated seeds lead to very low seeding density.

3. CONCLUSIONS

The ζ potentials of both Ga-face and N-face GaN grown on sapphire as a function of pH were measured. Both surfaces show negative ζ potential between pH 5.5 and 9. The N-face GaN has a more negative ζ potential, and on the basis of earlier studies by other groups, this is most likely due to higher concentration of adsorbed oxygen on the surface. The Ga-face shows an isoelectric point at ~pH 5.5. The results from the ζ potential study confirm the need for H-terminated seed solution at pH 8 to drive the self-assembly of a nanodiamond monolayer on the GaN surface. AFM studies on seeded Ga-face and N-face GaN confirmed the high seeding density when the surfaces were treated with H-terminated seeds. The subsequent growth of thin diamond films on the seeded wafers resulted in a pinhole-free diamond layer on the surface treated with H-terminated seeds for both orientations of GaN. This technique of growing diamond directly on GaN removes the need for a seeding layer like silicon nitride with low thermal conductivity.

4. EXPERIMENTAL SECTION

The results presented in this article consider Ga-face and N-face GaN. The two different orientations were fabricated by using samples grown by the complementary techniques of metal organic chemical vapor deposition and molecular beam epitaxy (MBE), which are known to generate Ga-face and N-face layers, respectively, for standard growth conditions. Both samples were grown on to 2 in. sapphire substrates, with the Ga-face samples produced in a Thomas Swan close-coupled showerhead 6 × 2 in. system, using trimethygallium and ammonia (NH_3) as sources. The details of the growth method are given in Bakshi et al.[31] For the N-polar samples, growth was carried out in a VG V80H MBE system with an SVTA nitrogen plasma source. The wafers were first degassed at 450 °C eurotherm for 24 h prior to entering the growth system to reduce contamination. Sample growths were carried out using 1 sccm of nitrogen gas flow and a plasma power of 350 W. A 20 min surface nitridation was carried out on the substrate surface at 750 ± 30 °C (measured by optical pyrometry, using a 50 nm layer of IR-absorbing molybdenum deposited on the back of the wafers prior to growth). The GaN was then deposited with a Ga flux of 17 nA and a growth time of 1 h 30 min to give a layer thickness of approximately 600 nm.

The streaming potential for both types of wafers were measured using a SurPASS 3 electrokinetic analyzer. The streaming potential is determined by measuring the change in potential or current between two Ag/AgCl electrodes at either end of a streaming channel as a function of the electrolyte pressure. The electrolyte flowing through the narrow channel shears the counterions from the charged surfaces in contact with the liquid. The flowing charge will create a streaming current across two electrodes positioned tangential to the flow. With the flow of counterions dependent on the electric double layer of the surfaces, measurement of the voltage then allows determination of the ζ potential. Streaming potential measurements have thus been used to determine the ζ potential of fibers.[32] For the measurement of streaming potential on flat surfaces meanwhile, a setup was suggested by Van Wagenen et al.[33] and has been successfully used by many authors for measurement on various flat surface geometries.[34−37] The streaming channel was formed between two plates of Ga-face or N-face wafers placed parallel to each other at a distance between 90 and 110 μm, and a 10^{-3} M solution of potassium chloride was used as the electrolyte and the pressure varied from 600 to 200 mbar. The pH of the electrolyte was then altered with 0.1 M HCl and 0.1 M NaOH solutions using the inbuilt titrator in SurPASS 3.

Seeding was carried out with monodispersed diamond/H_2O solutions in an ultrasonic bath, known to produce nucleation densities in excess of 10^{11} cm^{-2} atop silicon wafers.[38] Two types of solutions were used with both the wafers, one containing particles which were hydrogen-terminated and the other containing particles with oxygen termination. Although commercially available nanodiamond particles are oxygen terminated,[39] the process for hydrogen[40] termination of nanodiamond particles is detailed elsewhere. The oxygen- and hydrogen-terminated particles have negative and positive ζ potential in water, respectively. The particle size as indicated by dynamic light scattering was found to be approximately 7 nm for both of the seeding solutions used. To investigate the seeding density of the samples, atomic force microscopy (AFM) images were taken using Veeco Dimension 3100 equipped with RTESP tips (Bruker-Nano supplied, 8 nm nominal radius) in tapping mode. Post-AFM, analysis was carried out with WSXM[41] and Gwyddion[42] scanning probe microscopy analysis software. Scanning electron microscopy (SEM) images were taken using a Raith e-line operating at 20 kV and 10 mm working distance.

For the growth of diamond on GaN on sapphire, the samples were diced into 15 × 15 mm^2 pieces and seeded. The seeded wafers were then placed in a Seki Technotron AX6500X microwave chemical vapor deposition system for diamond growth. Growth was carried under 5% CH_4/H_2 condition at 40 Torr pressure and 3.5 kW microwave power. After growth, the samples were cooled slowly in hydrogen atmosphere to prevent cracking of the sapphire substrate. The growth of diamond on GaN was carried out on both the Ga-face and N-face of GaN.

AUTHOR INFORMATION

Corresponding Authors

*E-mail: mandals2@cardiff.ac.uk (S.M.).
*E-mail: williamso@cardiff.ac.uk (O.A.W.).

ORCID

Soumen Mandal: 0000-0001-8912-1439
Evan L. H. Thomas: 0000-0002-8580-7385
Laia Gines: 0000-0001-9980-054X
James T. Griffiths: 0000-0002-1198-1372

Notes

The authors declare no competing financial interest.

ACKNOWLEDGMENTS

This project has been supported by Engineering and Physical Sciences Research Council under program Grant GaN-DaME

DOI: 10.1021/acsomega.7b01069
ACS Omega 2017, 2, 7275−7280

(EP/P00945X/1). D.J.W. would like to acknowledge the support of EPSRC Manufacturing fellowship EP/N01202X/1. L.E.G. would like to acknowledge the support of Royal Society starting grant "SCOPE". Information on the data underpinning the results presented here, including how to access them, can be found in the Cardiff University data catalog at http://doi.org/10.17035/d.2017.0038570276.

REFERENCES

(1) Mishra, U. K.; Parikh, P.; Wu, Y.-F. AlGaN/GaN HEMTs—an overview of device operation and applications. *Proc. IEEE* **2002**, *90*, 1022−1031.
(2) Mishra, U. K.; Likun, S.; Kazior, T. E.; Wu, Y.-F. GaN-Based RF Power Devices and Amplifiers. *Proc. IEEE* **2008**, *96*, 287−305.
(3) Lee, S.; Vetury, R.; Brown, J. D.; Gibb, S. R.; Cai, W. Z.; Sun, J.; Green, D. S.; Shealy, J. In *Reliability Assessment of AlGaN/GaN HEMT Technology on SiC for 48V Applications*, 2008 IEEE International Reliability Physics Symposium, 2008; pp 446−449.
(4) Gaska, R.; Osinsky, A.; Yang, J. W.; Shur, M. S. Self-heating in high-power AlGaN-GaN HFET's. *IEEE Electron Device Lett.* **1998**, *19*, 89−91.
(5) Kuball, M.; Hayes, J. M.; Uren, M. J.; Martin, I.; Birbeck, J. C. H.; Balmer, R. S.; Hughes, B. T. Measurement of Temperature in Active High-Power AlGaN/GaN HFETs Using Raman Spectroscopy. *IEEE Electron Device Lett.* **2002**, *23*, 7−9.
(6) Goldberg, Y.; Levinshtein, M.; Rumyantsev, S. In *Properties of Advanced Semiconductor Materials GaN, AlN, SiC, BN, SiC, SiGe*; Levinshtein, M., Rumyantsev, S., Shur, M., Eds.; John Wiley & Sons, Inc.: New York, NY, 2001; pp 93−148.
(7) Ho, C. Y.; Powell, R. W.; Liley, P. E. Thermal Conductivity of the Elements. *J. Phys. Chem. Ref. Data* **1972**, *1*, 279−421.
(8) Jessen, G. H.; Gillespie, J. K.; Via, G. D.; Crespo, A.; Langley, D.; Wasserbauer, J.; Faili, F.; Francis, D.; Babic, D.; Ejeckam, F.; Guo, S.; Eliashevich, I. In *AlGaN/GaN HEMT on Diamond Technology Demonstration*, Technical Digest − IEEE Compound Semiconductor Integrated Circuit (CSIC) Symposium, 2006; pp 271−274.
(9) Hirama, K.; Taniyasu, Y.; Kasu, M. AlGaN/GaN high-electron mobility transistors with low thermal resistance grown on single-crystal diamond (111) substrates by metalorganic vapor-phase epitaxy. *Appl. Phys. Lett.* **2011**, *98*, No. 162112.
(10) Dumka, D. C.; Chou, T. M.; Jimenez, J. L.; Fanning, D. M.; Francis, D.; Faili, F.; Ejeckam, F.; Bernardoni, M.; Pomeroy, J. W.; Kuball, M. In *Electrical and Thermal Performance of AlGaN/GaN HEMTs on Diamond Substrate for RF Applications, 2013 IEEE Compound Semiconductor Integrated Circuit Symposium (CSICS)*, 2013; pp 14.
(11) Pomeroy, J. W.; Bernardoni, M.; Dumka, D. C.; Fanning, D. M.; Kuball, M. Low thermal resistance GaN-on-diamond transistors characterized by three-dimensional Raman thermography mapping. *Appl. Phys. Lett.* **2014**, *104*, No. 083513.
(12) Coe, S. E.; Sussmann, R. S. Optical, thermal and mechanical properties of CVD diamond. *Diamond Relat. Mater.* **2000**, *9*, 1726−1729.
(13) Sun, H.; Simon, R. B.; Pomeroy, J. W.; Francis, D.; Faili, F.; Twitchen, D. J.; Kuball, M. Reducing GaN-on-diamond interfacial thermal resistance for high power transistor applications. *Appl. Phys. Lett.* **2015**, *106*, No. 111906.
(14) Gu, X.; Lee, C.; Xie, J.; Beam, E.; Becker, M.; Grotjohn, T. A.; Anaya, J.; Kuball, M. In *GaN-on-Diamond with Ultra-Low Thermal Barrier Resistance*, GOMAC Tech 2016, 2016; pp 405−408.
(15) Zhou, Y.; Ramaneti, R.; Anaya, J.; Korneychuk, S.; Derluyn, J.; Sun, H.; Pomeroy, J.; Verbeeck, J.; Haenen, K.; Kuball, M. Thermal characterization of polycrystalline diamond thin film heat spreaders grown on GaN HEMTs. *Appl. Phys. Lett.* **2017**, *111*, No. 041901.
(16) Zhou, Y.; Anaya, J.; Pomeroy, J.; Sun, H.; Gu, X.; Xie, A.; Beam, E.; Becker, M.; Grotjohn, T.; Lee, C.; Kuball, M. Barrier Layer Optimization for Enhanced GaN-ondiamond Device Cooling. *ACS Appl. Mater. Interfaces* **2017**, *9*, 34416−34422.
(17) Harkins, W. D. Energy Relations of the Surface of Solids I. Surface Energy of the Diamond. *J. Chem. Phys.* **1942**, *10*, 268−272.
(18) Jaccodine, R. J. Surface Energy of Germanium and Silicon. *J. Electrochem. Soc.* **1963**, *110*, 524.
(19) Northrup, J. E.; Neugebauer, J. Theory of GaN($10\bar{1}0$) and ($11\bar{2}0$) surfaces. *Phys. Rev. B* **1996**, *53*, No. R10477.
(20) Williams, O. A. Nanocrystalline diamond. *Diamond Relat. Mater.* **2011**, *20*, 621−640.
(21) Hellman, E. S.; Buchanan, D. N. E.; Wiesmann, D.; Brener, I. Growth of Ga-face and N-face GaN films using ZnO Substrates. *MRS Internet J. Nitride Semicond. Res.* **1996**, *1*, No. e16.
(22) Zywietz, T. K.; Neugebauer, J.; Scheffler, M. The adsorption of oxygen at GaN surfaces. *Appl. Phys. Lett.* **1999**, *74*, 1695−1697.
(23) Tarsa, E. J.; Heying, B.; Wu, X. H.; Fini, P.; DenBaars, S. P.; Speck, J. S. Homoepitaxial growth of GaN under Ga-stable and N-stable conditions by plasma-assisted molecular beam epitaxy. *J. Appl. Phys.* **1997**, *82*, 5472−5479.
(24) Foster, C. M.; Collazo, R.; Sitar, Z.; Ivanisevic, A. Aqueous stability of Ga- and N-polar gallium nitride. *Langmuir* **2013**, *29*, 216−220.
(25) Chingombe, P.; Saha, B.; Wakeman, R. J. Surface modification and characterisation of a coal-based activated carbon. *Carbon* **2005**, *43*, 3132−3143.
(26) Uhlrich, J. J.; Grabow, L. C.; Mavrikakis, M.; Kuech, T. F. Practical Surface Treatments and Surface Chemistry of n-Type and p-Type GaN. *J. Electron. Mater.* **2008**, *37*, 439−447.
(27) Hees, J.; Kriele, A.; Williams, O. A. Electrostatic self-assembly of diamond nanoparticles. *Chem. Phys. Lett.* **2011**, *509*, 12−15.
(28) Girard, H. A.; Perruchas, S.; Gesset, C.; Chaigneau, M.; Vieille, L.; Arnault, J.-C.; Bergonzo, P.; Boilot, J.-P.; Gacoin, T. Electrostatic grafting of diamond nanoparticles: A versatile route to nanocrystalline diamond thin films. *ACS Appl. Mater. Interfaces* **2009**, *1*, 2738−2746.
(29) Spitsyn, B. V.; Bouilov, L. L.; Derjaguin, B. V. Vapor growth of diamond on diamond and other surfaces. *J. Cryst. Growth* **1981**, *52*, 219−226.
(30) Dennig, P. A.; Stevenson, D. A. Influence of substrate topography on the nucleation of diamond thin films. *Appl. Phys. Lett.* **1991**, *59*, 1562−1564.
(31) Bakshi, S. D.; Sumner, J.; Kappers, M. J.; Oliver, R. A. The influence of coalescence time on unintentional doping in GaN/sapphire. *J. Cryst. Growth* **2009**, *311*, 232−237.
(32) Jacobasch, H.-J.; Bauböck, G.; Schurz, J. Problems and results of zeta-potential measurements on fibers. *Colloid Polym. Sci.* **1985**, *263*, 3−24.
(33) Van Wagenen, R. A.; Andrade, J. D. Flat plate streaming potential investigations: Hydrodynamics and electrokinetic equivalency. *J. Colloid Interface Sci.* **1980**, *76*, 305−314.
(34) Voigt, A.; Wolf, H.; Lauekner, S.; Neumann, G.; Becker, R.; Richter, L. Electrokinetic properties of polymer and glass surfaces in aqueous solutions: Experimental evidence for swollen surface layers. *Biomaterials* **1983**, *4*, 299−304.
(35) Norde, W.; Rouwendal, E. Streaming potential measurements as a tool to study protein adsorption kinetics. *J. Colloid Interface Sci.* **1990**, *139*, 169−176.
(36) Scales, P. J.; Grieser, F.; Healy, T. W. Electrokinetics of the muscovite mica-aqueous solution interface. *Langmuir* **1990**, *6*, 582−589.
(37) Werner, C.; Jacobasch, H.-J.; Reichelt, G. Surface characterization of hemodialysis membranes based on streaming potential measurements. *J. Biomater. Sci., Polym. Ed.* **1996**, *7*, 61−76.
(38) Williams, O. A.; Douhéret, O.; Daenen, M.; Haenen, K.; Ōsawa, E.; Takahashi, M. Enhanced diamond nucleation on monodispersed nanocrystalline diamond. *Chem. Phys. Lett.* **2007**, *445*, 255−258.
(39) Mochalin, V. N.; Shenderova, O.; Ho, D.; Gogotsi, Y. The properties and applications of nanodiamonds. *Nat. Nanotechnol.* **2011**, *7*, 11−23.
(40) Williams, O. A.; Hees, J.; Dieker, C.; Jäger, W.; Kirste, L.; Nebel, C. E. Size-Dependent Reactivity of Diamond Nanoparticles. *ACS Nano* **2010**, *4*, 4824−4830.

DOI: 10.1021/acsomega.7b01069
ACS Omega 2017, 2, 7275−7280

(41) Horcas, I.; Fernández, R.; Gómez-Rodríguez, J. M.; Colchero, J.; Gómez-Herrero, J.; Baro, A. M. WSXM: A software for scanning probe microscopy and a tool for nanotechnology. *Rev. Sci. Instrum.* **2007**, *78*, No. 013705.
(42) Nečas, D.; Klapetek, P. Gwyddion: an open-source software for SPM data analysis. *Cent. Eur. J. Phys.* **2012**, *10*, 181.

DOI: 10.1021/acsomega.7b01069
ACS Omega 2017, 2, 7275−7280